SUPPLEMENTAL MATERIAL

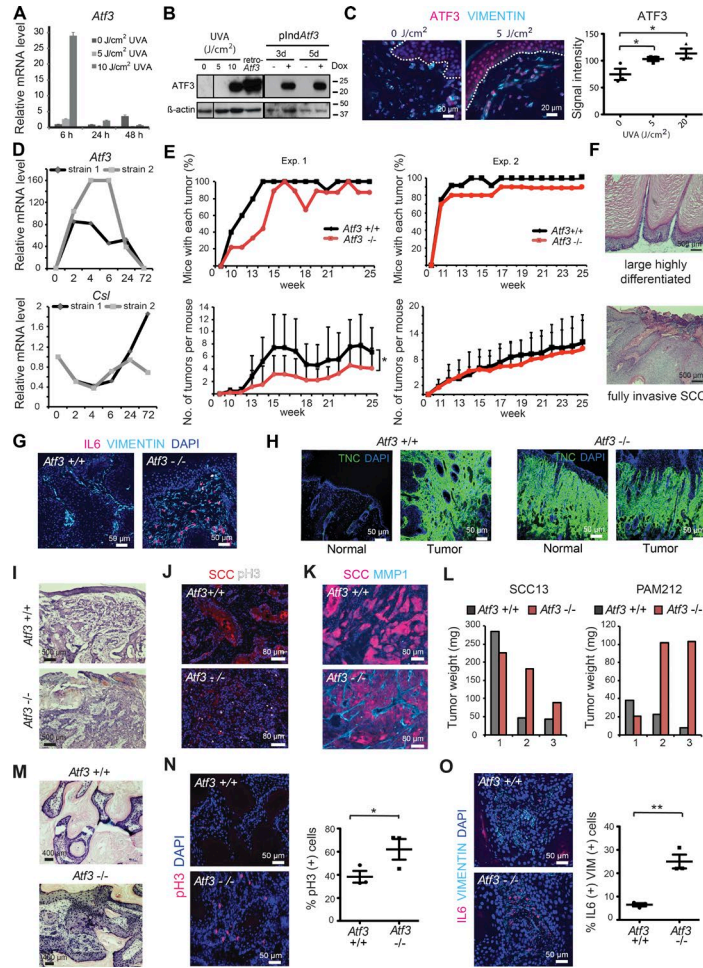**Kim et al., https://doi.org/10.1084/jem.20170724**

Figure S1. **ATF3 deficiency promotes dysplastic keratinocyte tumors and CAF activation.** (A) HDFs were treated with UVA at the indicated doses, followed, at the indicated times (hours), by RT-qPCR analysis of *Atf3* expression, with *36β4* for normalization. Data are mean ± SD. (B) HDFs were treated with UVA at the indicated doses and analyzed 6 h after irradiation in parallel with HDFs infected with a constitutive ATF3-expressing retrovirus (ATF3 retro) or with a lentivirus for doxycycline-inducible ATF3 expression (pInd-*Atf3*; 3 and 5 d after doxycycline treatment) for ATF3 protein levels by immunoblotting. (C) Human skin explants, 24 h after being placed in the culture, were mock treated or treated with UVA at the indicated dose, followed 6 h later by double IF analysis with Ab against ATF3 and vimentin for fibroblast identification. Shown is a representative image and quantification of the mean ATF3 fluorescence signal per vimentin-positive cell using the lasso tool in Adobe Photoshop. n = 3 fields per condition, mean ± SEM, one-tailed unpaired *t* test, *, P < 0.05. (D) Two independent HDF strains were treated with UVA 5J/cm², followed, at the indicated times (hours), by RT-qPCR analysis of *Atf3* and *Csl* expression, with *36β4* for normalization. (E) Time of appearance, incidence, and number of skin tumors in two independent experiments of multistep chemical carcinogenesis with mice with and without ATF3 gene deletion over 25 wk. The results of the histological and IF analysis are shown in Fig. 1 (D–I). n = 10 *Atf3*^+/+^ and n = 9 *Atf3*^−/−^ mice in the first experiment, n = 8 *Atf3*^+/+^ and n = 9 *Atf3*^−/−^ mice for the second experiment. Mean ± SD, one-tailed unpaired *t* test, *, P < 0.05. (F) Representative histological images of highly differentiated papillomas, not found in mice with *Atf3* gene deletion, and invasive SCCs, which did not develop in control mice within the period of the experiments (25 wk). (G) Additional representative images in addition to those shown in Fig. 1 H, of IL6/vimentin double IF analysis of tumors formed in *Atf3*^−/−^ versus +/+ mice. (H) Additional representative images, in addition to those shown in Fig. 1 I, of TNC IF analysis of tumors formed in *Atf3*^−/−^ versus +/+ mice versus matching distant normal skin region. (I) Additional representative H&E images of another pair of ear lesions in addition to that shown in Fig. 2 E formed after injection of SCC13 cells admixed with dermal fibroblasts with and without *Atf3* deletion. (J) Representative images of IF analysis of ear lesions with anti-phospho-histone 3 Ab (pH3, white) using red fluorescence signal for identification of DsRed2-expressing SCC13 cells (SCC). (K) Additional representative images, in addition to those shown in Fig. 2 G, of IF analysis of ear lesions with Ab against MMP1 using DsRed2 signal for SCC cell identification. (L and M) Weakly tumorigenic mouse PAM212 keratinocytes or SCC13 cells were admixed with mouse dermal fibroblasts with or without *Atf3* deletion followed by parallel intradermal injections in NOD/SCID mice. Three mice per condition were injected. Shown are the weights of tumors at the end of the experiment (4 wk for SCC13, 8 wk for PAM212; L) as well as representative histological images (M). (N) Shown are representative images (left panels) and quantification (right panel) of pH3 IF analysis in intradermal lesions. n = 3 lesion per condition, n = 6 fields per lesion, mean ± SEM, one-tailed paired *t* test, *, P < 0.05. (O) Representative images of double IF analysis of tumors with anti-IL6 and anti-vimentin Ab (left panels) and relative quantification (right panel). n = 3 lesion per condition, three to six fields per lesion, mean ± SEM, two-tailed unpaired *t* test, **, P < 0.005.
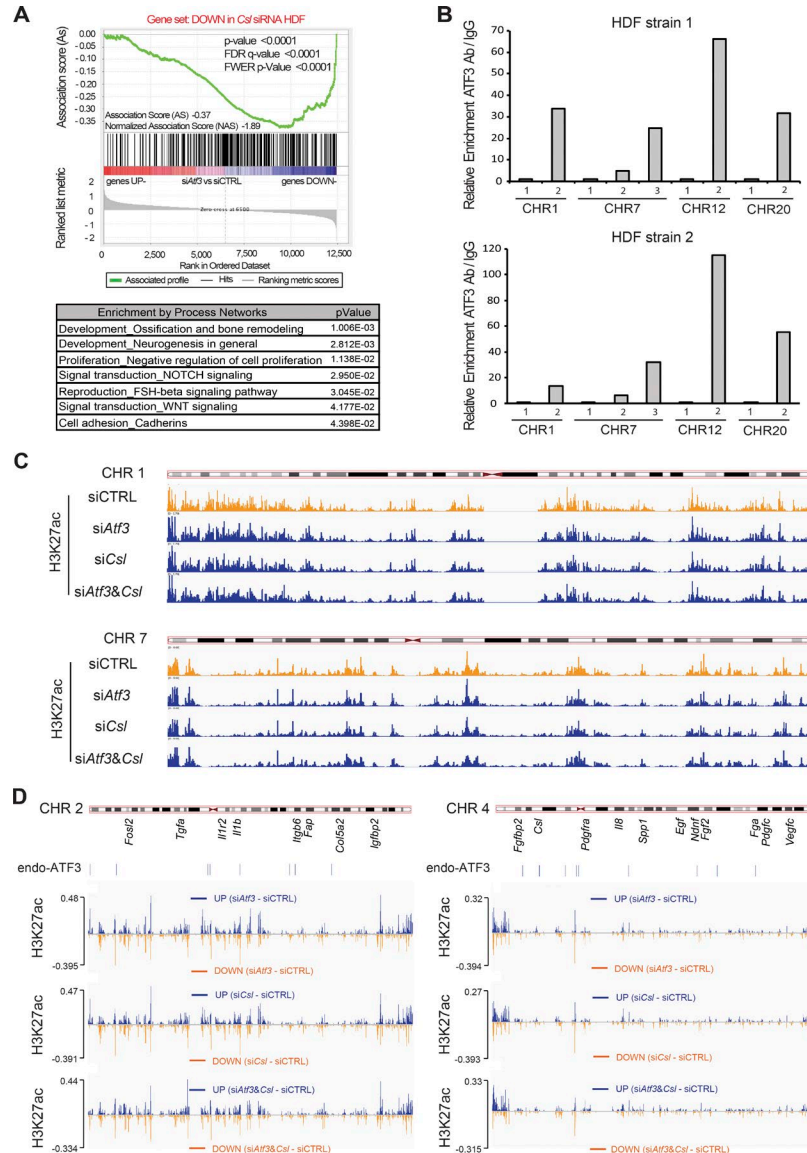
Figure S2. ***Atf3* and *Csl* gene silencing cause similar changes in transcriptional profile and global chromatin configuration.** (A, top) Plot for gene set enrichment analysis (GSEA) using RNA-seq expression profiles of two HDF strains with and without silencing of *Atf3* by two different siRNAs against genes down-modulated in HDF by Csl silencing (Procopio et al., 2015). Genes are ranked by signal-to-noise ratio based on their differential expression in control versus *Atf3*-silenced HDFs; position of genes in the CSL gene set is indicated by black vertical bars, and the enrichment score is shown in green. (A, bottom) List of process networks with statistically significant enrichment ($P < 0.05$) as identified by GeneGo MetaCore analysis of genes within the core enrichment of GSE analysis in the left panel. The complete list of processes and corresponding genes is provided in Table S5. (B) ChIP assays for independent confirmation of ChIP-seq results of binding of low levels of *Atf3* to specific genomic regions (as shown in Fig. 5 B and Fig. S3, A–C). Two different HDF strains were processed for ChIP assays by immune precipitation with anti-ATF3 Ab versus nonimmune IgGs followed by "tagmentation" for signal amplification (see Method and materials). qPCR analysis of specific sites expected to bind ATF3 versus nonbinding was as follows: chr 1, site 1 (nonbinding; 149813681–149813502), site 2 (ATF3 binding upstream of the *Hist2h3d* gene; 149662083–149662513); chr 7, site 1 (nonbinding; 52527334–52527468), site 2 (ATF3 binding upstream of the *Hoxa9* gene; 26653219–26653625), site 3 (ATF3 binding upstream of the *Il6* gene; 20756656–20757004); chr 12, site 1 (nonbinding; 2707117–2706912), site 2 (ATF3 binding upstream of the *Tead4* gene; 2852607–2852995); and chr 20, site 1 (nonbinding, 30390343–30390564), site 2 (ATF3 binding upstream of the *Id1* gene; 29637665–29638087). Values are expressed as enrichment folds of bound sequences in the ATF3 immune precipitates versus nonimmune IgGs. (C) The individual pattern of H3K27ac along the entire length of the two chromosomes (CHR 1 and 7) is shown as differences in Fig. 5 A from HDFs with silencing of *Atf3* (si*Atf3*) and *Csl* (si*Csl*), individually and in combination, relative to control cells (siCtrl). (D) Difference in H3K27 acetylation along the entire length of two other chromosomes (CHR 2 and 4) in HDFs with silencing of *Atf3* (si*Atf3*) and *Csl* (si*Csl*), individually and in combination (si*Atf3*+si*Csl*), relative to control cells (siCtrl), as calculated and visualized by IGV subtract operator tool to combine data tracks. The approximate locations of individual CAF-related genes are shown below the chromosomal maps. The location of the endogenous ATF3 binding position, as assessed by ChIP-seq and calculated by MACS (Table S6), is shown below the chromosomal maps.
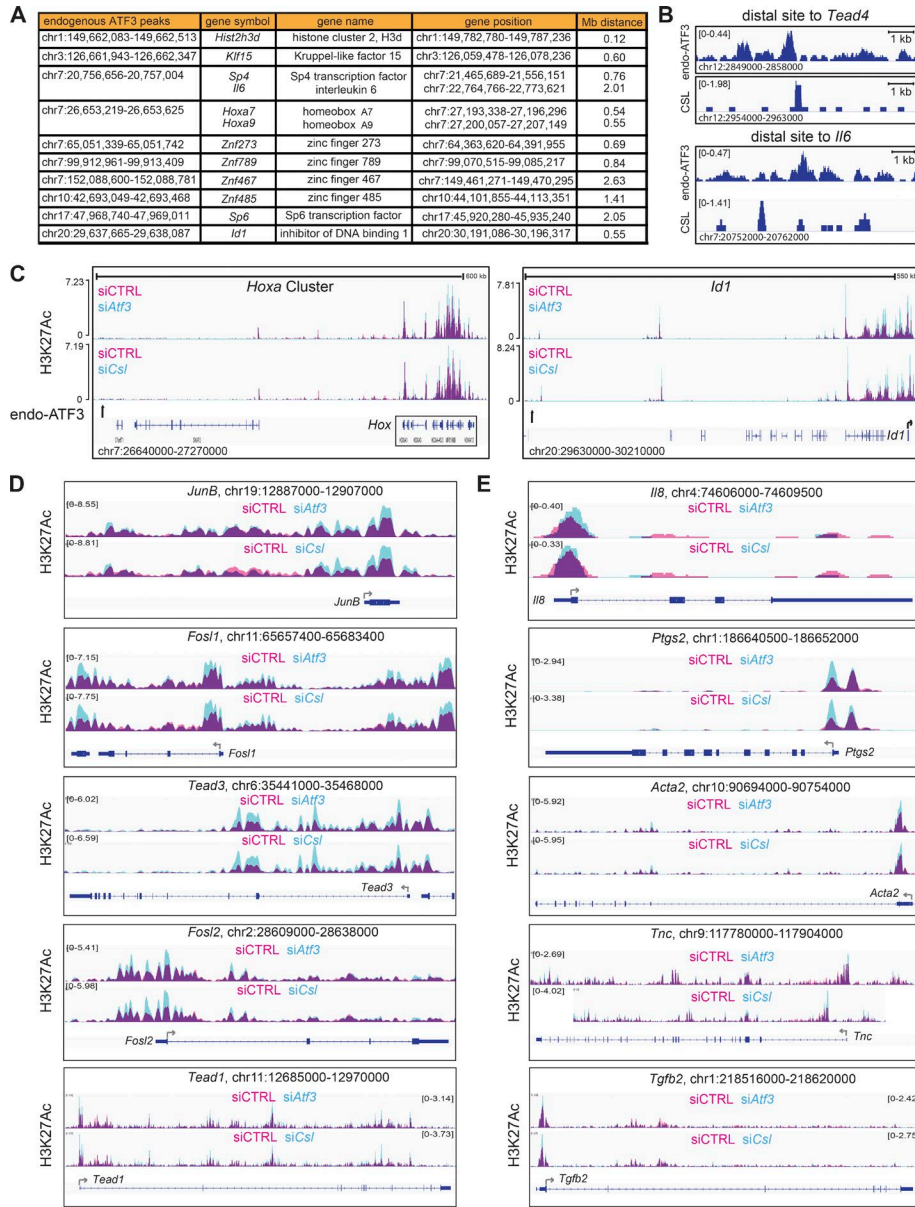
A

endogenous ATF3 peaks	gene symbol	gene name	gene position	Mb distance
chr1:149,662,083-149,662,513	Hist2h3d	histone cluster 2, H3d	chr1:149,782,780-149,787,236	0.12
chr3:126,661,943-126,662,347	Klf15	Kruppel-like factor 15	chr3:126,059,478-126,078,236	0.60
chr7:20,756,656-20,757,004	Sp4	Sp4 transcription factor	chr7:21,465,689-21,556,151	0.76
	Il6	interleukin 6	chr7:22,764,766-22,773,621	2.01
chr7:26,653,219-26,653,625	Hoxa7	homeobox A7	chr7:27,193,338-27,196,296	0.54
	Hoxa9	homeobox A9	chr7:27,200,057-27,207,149	0.55
chr7:65,051,339-65,051,742	Znf273	zinc finger 273	chr7:64,363,620-64,391,955	0.69
chr7:99,912,961-99,913,409	Znf789	zinc finger 789	chr7:99,070,515-99,085,217	0.84
chr7:152,088,600-152,088,781	Znf467	zinc finger 467	chr7:149,461,271-149,470,295	2.63
chr10:42,693,049-42,693,468	Znf485	zinc finger 485	chr10:44,101,855-44,113,351	1.41
chr17:47,968,740-47,969,011	Sp6	Sp6 transcription factor	chr17:45,920,280-45,935,240	2.05
chr20:29,637,665-29,638,087	Id1	inhibitor of DNA binding 1	chr20:30,191,086-30,196,317	0.55

Figure S3. ***Atf3*** **and** ***Csl*** **gene silencing cause similar chromatin changes at genomic loci to which endogenous ATF3 does not bind.** (A) Position and distance of endogenous ATF3 binding sites and flanking genes with transcription regulatory functions. Out of the ATF3-modulated genes shown in Fig. 4 D, shown are those localized within 2 Mb from endogenous ATF3 binding sites. (B) "Zoomed in" ATF3 and CSL binding sites as calculated by MACS (Table S6 and previously reported in Procopio et al., 2015) of the TEAD4 and IL6 loci are shown in Fig. 5 B. For each panel, the chromosomal locations of the shown loci and scale bars are depicted at the bottom and top, respectively. (C) Changes in H3K27 acetylation caused by *Atf3* or *Csl* silencing at chromosomal regions encompassing endogenous ATF3 binding sites and flanking HOXA cluster and ID-1 locus. For each panel, the chromosomal locations of the shown loci and scale bars are depicted at the bottom and top, respectively. Peaks of H3K27ac present in control HDFs (siCTRL) are shown in pink, peaks in HDFs with gene silencing for *Atf3* (si*Atf3*) or *Csl* (si*Csl*) are shown in turquoise, and overlapping areas present in both cells are shown in purple. Individual profiles for each condition were visualized in IGV and merged using Adobe Photoshop. ATF3 binding sites as calculated by MACS (Table S6) are indicated by vertical black arrows. Lower lines are transcribed and spliced regions (blue boxes = coding exons) as predicted by Ensembl, together with the position and direction of transcription start sites (arrows) for the *Id1* gene. For each panel, the chromosomal locations of the shown loci and scale bars are depicted at the bottom and top, respectively. (D and E) Shown are changes in H3K27 acetylation caused by *Atf3* or *Csl* silencing at various genomic loci, in addition to those shown in Fig. 5 C, coding for positive regulators (D) or effectors (E) of CAF function, to which endogenous ATF3 does not bind. Peaks of H3K27ac present in control HDFs (siCTRL) are shown in pink, peaks in HDFs with gene silencing for *Atf3* (si*Atf3*) or *Csl* (si*Csl*) are shown in turquoise, and overlapping areas present in both cells are shown in purple. Individual profiles for each condition were visualized in IGV and merged using Adobe Photoshop. Lower lines are transcribed and spliced regions (blue boxes = coding exons) as predicted by Ensembl, together with the position and direction of transcription start sites (arrows). The chromosomal locations of the shown loci are depicted at the top of each panel.
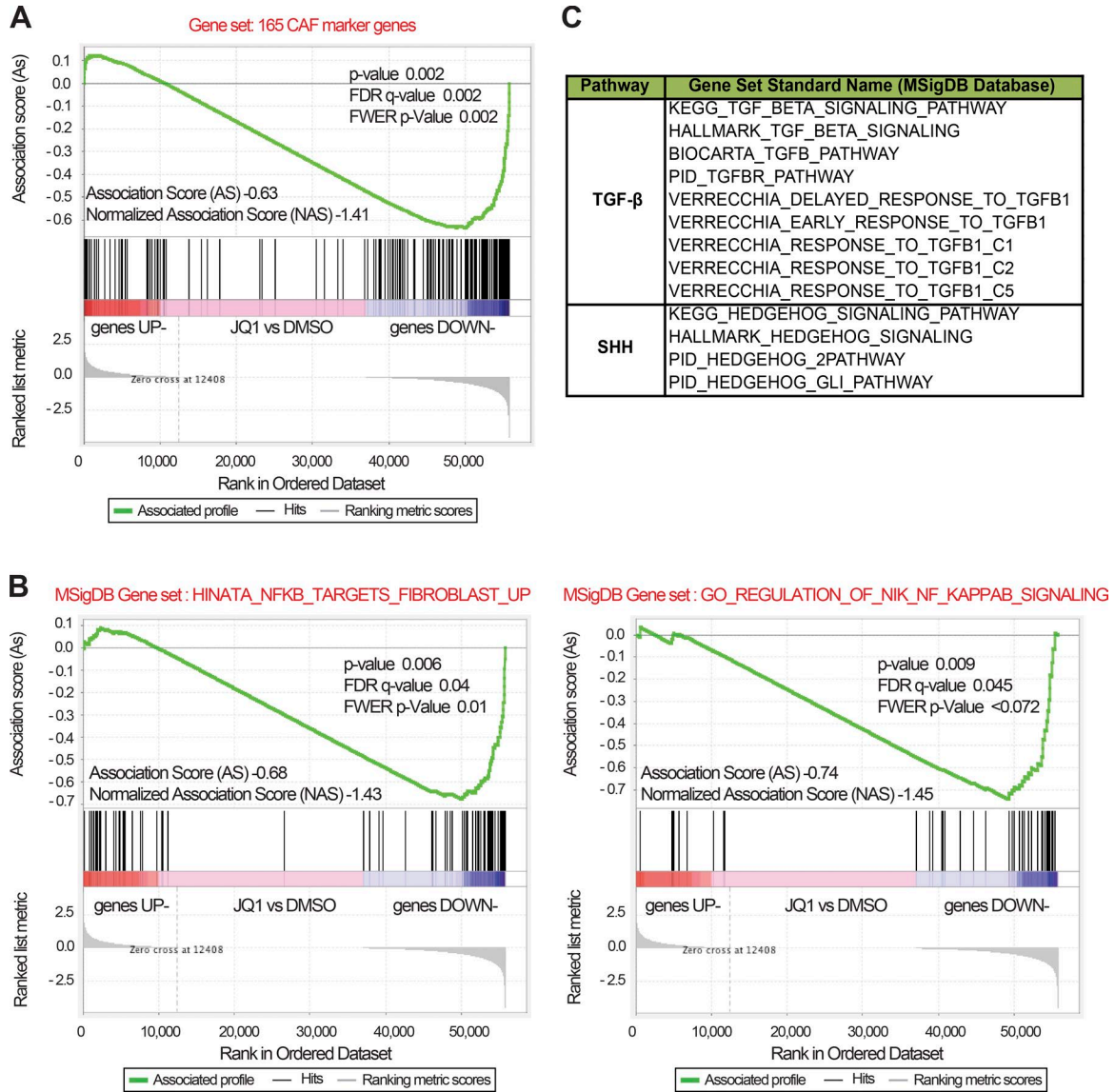
A

Gene set: 165 CAF marker genes

p-value 0.002
FDR q-value 0.002
FWER p-Value 0.002

Association Score (AS) -0.63
Normalized Association Score (NAS) -1.41

genes UP-   JQ1 vs DMSO   genes DOWN-

Zero cross at 12408

Rank in Ordered Dataset

— Associated profile — Hits — Ranking metric scores

C

Pathway	Gene Set Standard Name (MSigDB Database)
TGF-β	KEGG_TGF_BETA_SIGNALING_PATHWAY
	HALLMARK_TGF_BETA_SIGNALING
	BIOCARTA_TGFB_PATHWAY
	PID_TGFBR_PATHWAY
	VERRECCHIA_DELAYED_RESPONSE_TO_TGFB1
	VERRECCHIA_EARLY_RESPONSE_TO_TGFB1
	VERRECCHIA_RESPONSE_TO_TGFB1_C1
	VERRECCHIA_RESPONSE_TO_TGFB1_C2
	VERRECCHIA_RESPONSE_TO_TGFB1_C5
SHH	KEGG_HEDGEHOG_SIGNALING_PATHWAY
	HALLMARK_HEDGEHOG_SIGNALING
	PID_HEDGEHOG_2PATHWAY
	PID_HEDGEHOG_GLI_PATHWAY

B

MSigDB Gene set : HINATA_NFKB_TARGETS_FIBROBLAST_UP

p-value 0.006
FDR q-value 0.04
FWER p-Value 0.01

Association Score (AS) -0.68
Normalized Association Score (NAS) -1.43

genes UP-   JQ1 vs DMSO   genes DOWN-

Zero cross at 12408

Rank in Ordered Dataset

— Associated profile — Hits — Ranking metric scores

MSigDB Gene set : GO_REGULATION_OF_NIK_NF_KAPPAB_SIGNALING

p-value 0.009
FDR q-value 0.045
FWER p-Value <0.072

Association Score (AS) -0.74
Normalized Association Score (NAS) -1.45

genes UP-   JQ1 vs DMSO   genes DOWN-

Zero cross at 12408

Rank in Ordered Dataset

— Associated profile — Hits — Ranking metric scores

Figure S4. **JQ1–modulated genes are significantly correlated with NF-κB but not SHH or TGF-β–signaling gene sets.** (A) Plot of gene set enrichment analysis (GSEA) using RNA-seq expression profile of three CAF strains with and without JQ1 treatment (500 nM for 2 d) versus vehicle alone (DMSO) against a set of 165 CAF signature genes (Table S9). Genes are ranked by signal-to-noise ratio based on their differential expression in CAFs with JQ1 versus vehicle treatment; the positions of genes from the gene set are indicated by black vertical bars, and the enrichment score is shown in green. (B) Plot of GSEA using RNA-seq expression profile of three CAF strains with and without JQ1 treatment (500 nM for 2 d) versus vehicle alone (DMSO) against two different NF-κB signaling gene sets publicly available in the Molecular Signatures Database (MSigDB), one experimentally determined from a specific study of NF-κB activation in HDFs (left panel) and another based on a common gene signature from multiple studies (for the noncanonical pathway; right panel). Genes are ranked by signal-to-noise ratio based on their differential expression in CAFs with JQ1 versus vehicle treatment; the positions of genes from the gene set are indicated by black vertical bars, and the enrichment score is shown in green. (C) List of gene sets publicly available in the Molecular Signatures Database (MSigDB) for TGB-β and SHH pathways used for GSE analysis of the RNA-seq expression profiles of CAFs treated with JQ1.
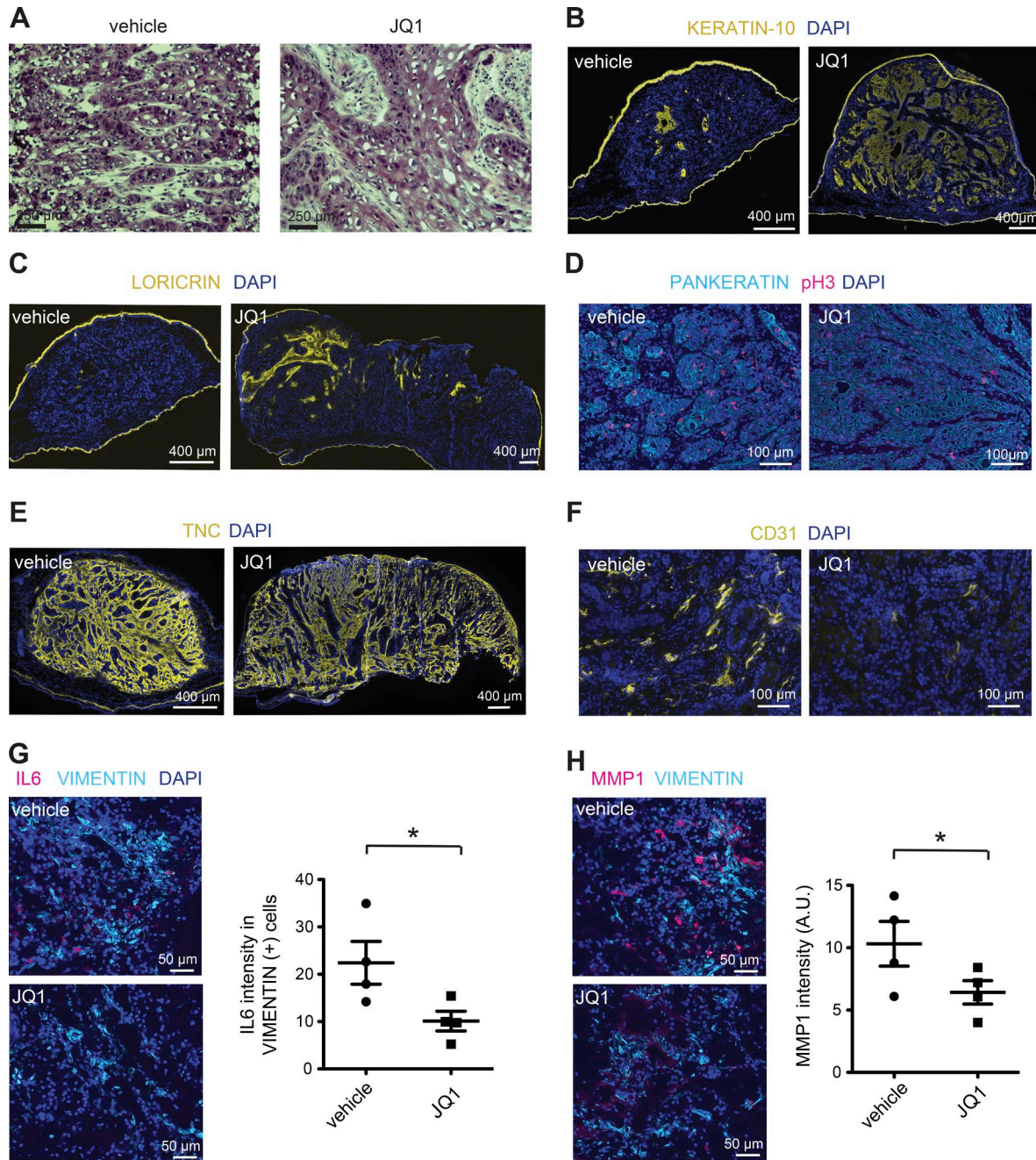
Figure S5. **BET inhibitor treatment promotes tumor squamous cell differentiation and suppresses expression of CAF–determinant genes in induced skin lesions and human skin SCC explants.** (A) Representative histological images of another pair of mouse ear lesions topically treated with JQ1 or DMSO vehicle alone as in Fig. 8 A. (B and C) Representative images of IF analysis with Ab against keratinocyte differentiation (keratin 10 [K10] and loricrin) markers of ear lesions topically treated with JQ1 or ethanol vehicle alone. (D) Representative images of IF analysis with Ab against proliferation markers (phospho-H3) and pankeratin Ab for tumor cell identification of ear lesions topically treated with JQ1 or DMSO vehicle alone. Quantification of the results is shown in Fig. 8 B. (E and F) Representative images of IF analysis with Ab against TNC and CD31 endothelial cell markers of ear lesions topically treated with JQ1 or ethanol vehicle alone different from those shown in Fig. 8 (E and F). (G and H) Skin SCC explants from four different patients maintained in semisolid agarose medium were treated daily with 500 nM JQ1 or DMSO vehicle alone, followed by double IF analysis with Ab against IL6 and vimentin (G) and against MMP1 and vimentin (H). IL6 signal intensity in vimentin-positive cells was quantified by Adobe Photoshop using the lasso function in three different fields from four paired skin SCC explants. MMP1 signal intensity was quantified by ImageJ software in three different fields from four paired explant tissues. $n = 4$ SCC lesions, mean ± SEM, one–tailed paired t test, *, P < 0.05.

Tables S1–S11 are shown as Excel files.

Table S1. Combined ChIP–seq and RNA–seq analysis of induced *Atf3* and *Csl* in HDF. Shown are (a) peak heights ("tags") and ratio of ATF3 binding to Input ("fold enrichment") as identified by the peak caller software MACS for induced ATF3 ChIP–seq; (b) peak positions from TSS of the most proximal gene for induced ATF3 binding sites as identified by ChIP–seq analysis; (c) a complete list of genes differentially expressed in HDFs with enhanced *ATF3* expression as identified by RNA–seq analysis; (d) a list of process networks identified by GeneGo MetaCore analysis and corresponding genes; (e) a list of genes as identified by ATF3 and CSL ChIP–seq analysis of HDFs with enhanced *ATF3* expression versus endogenous *CSL*; and (f) a list of RNA–seq profiles of HDFs with and without increased *ATF3* expression or with and without *CSL* gene silencing.

Table S2. GeneGo MetaCore analysis of ATF3/CSL–regulated target genes identified by ChIP–seq and RNA–seq. Shown is a list of process networks identified by GeneGo MetaCore analysis for (a) 662 regulated direct target genes of enhanced *Atf3* expression and (b) 102 common regulated target genes of induced ATF3 and CSL as identified by combined analysis of ChIP–seq and RNA–seq.

Table S3. Induced ATF3 and endogenous CSL binding peak positions on 102 common regulated target genes. Peak positions from TSS of the most proximal gene for induced *Atf3* and endogenous CSL binding sites as identified by ChIP–seq analysis.

Table S4. RNA–seq profiles of HDF with and without *Atf3* gene silencing. Shown are (a) a complete list of genes differentially expressed in two strains of primary HDFs 3 d after transfection with two different anti–*Atf3* siRNAs versus scrambled control; (b) a list of process networks identified by GeneGo MetaCore analysis and corresponding genes; and (c) a list of common process networks affected by both increased and suppressed ATF3 expression.

Table S5. GeneGo MetaCore analysis for gene set enrichment analysis (GSEA) of *Atf3*–silenced HDFs. Shown are a list of process networks identified by GeneGo MetaCore analysis for genes within the core enrichment (leading–edge subset) of GSEA for the HDF with and without *Atf3*–silencing RNA–seq profile against the gene set for (a) genes up–modulated or (b) down–regulated by *Csl* silencing, as shown in Fig. 4 D and Fig. S4 A, respectively.

Table S6. ChIP–seq profile of endogenous ATF3 in HDF. Shown are (a) the peak heights ("tags") and ratio of ATF3 binding to Input ("fold enrichment") as identified by the peak caller software MACS for endogenous ATF3 ChIP–seq; (b) a list of 128 ensemble IDs identified by ATF3 ChIP–seq analysis of HDFs under basal conditions and corresponding peaks; and (c) a list of 60 overlapping target and corresponding peaks bound by endogenous ATF3 and CSL in HDFs as identified by ChIP–seq analysis.

Table S7. RNA–seq profiles of CAFs with and without JQ1 treatment. Shown are (a) a complete list of genes differentially expressed in three strains of primary CAFs treated with JQ1 (500 nM) versus DMSO vehicle and (b) a list of process networks identified by GeneGo MetaCore analysis for genes up– or down–modulated upon JQ1 treatment.

Table S8. GeneGo MetaCore analysis for gene set enrichment analysis (GSEA) of JQ1–treated CAFs. Shown is a list of process networks identified by GeneGo MetaCore analysis for genes within the core enrichment (leading–edge subset) of GSEA for JQ1–treated CAFs RNA–seq profiles against the gene set for (a) genes down–modulated by induced *Atf3*; (b) genes up–regulated by *Atf3* siRNA knockdown; and (c) genes up–regulated by *Csl* siRNA knockdown, as shown in Fig. 7 (A–C).

Table S9. CAF gene set used for GSE analysis. Shown are 165 signature genes bearing on various aspects of CAF activation as identified from a literature search.

Table S10. RT–qPCR primers, guide RNAs, and siRNAs used in this study.

Table S11. Antibodies used in this study.